Modeling of Bolts using the GISSMO Model for Crash Analysis

Florian Schauwecker[1, 2], David Moncayo[1], Dr. Filipe Andrade[3], Dr.-Ing. Markus Feucht[1], Dr.-Ing. Markus Beck[1], Prof. Dr.-Ing. Peter Middendorf[2]

[1] *Daimler AG, Research and Development, Sindelfingen, Germany*
[2] *IFB Institute of Aircraft Design, University of Stuttgart, Germany*
[3] *DYNAmore GmbH, Stuttgart, Germany*

1 Introduction

The prediction accuracy of bolted connections is becoming increasingly important in the automotive sector. The requirements and thus the vehicle architectures are changing due to the electrification of vehicles and the high weight of batteries as well as their low permissible intrusion depth. Bolts are required as detachable fasteners to connect batteries with the body in white. The energy absorption concepts of vehicles with internal combustion engines have been continuously developed over the past decades. Thanks to many years of experience, the bolt connection behavior and load transfer are well known. Energy absorption concepts for electrically powered vehicles are in a comparatively early development phase. For the evaluation and further development of new crash concepts, a reliable simulation method is a basic requirement to predict joint failure in bolted connections.
Sonnenschein [1]; Hadjioannou, Stevens and Barsotti [2] and Narkhede et al [3] investigated the bolt behavior under static and dynamic loads. Beam elements represent the bolt shanks in numerical investigations with LS-DYNA. Those modeling techniques are numerical efficient, suitable for the application in full vehicle crash simulations and easily evaluable in post processing processes. However, their force or strain-based failure criteria only take damage as an approximation over a bi- or multilinear progression into account. Further, an accurate modeling is necessary to obtain the intended force transmission and to correctly consider pre-tension.
Fransplass et al. [4, 5] investigate the failure behavior of M5 threaded rods with a property class of 4.6 under static and dynamic loads. They use a detailed model with hexahedral solid elements and an average mesh size of 0.075 mm for their numerical investigations. The thermoelastic-thermoviscoplastic constitutive model **`*MAT_107,`** implemented in LS-DYNA, describes the damage and failure behavior.
Schauwecker et al. [6] show the importance of the distinction between the thread and the shank based on experimental investigations under tensile, shear and combined loads. In their numerical model with an average element length of 0.5 mm, a variation of the cross-sectional area considers the thread geometrically. The nominal bolt diameter applies to the shank, whereas the stress cross-sectional diameter applies to the threaded part of the bolt. In an additional publication, Schauwecker et al. [7] indicate what needs to be considered for a coarse bolt modeling which is suitable for a full vehicle simulation, with regards to the cross-sectional area. These results are generated with an already existing material card, from the Daimler material data base, validated for a complex phase steel CP1000, whose material properties correspond with the requirements of the standard DIN EN ISO 898-1 [8] for 10.9 bolts.

This paper presents a novel discretization approach with a new method to adapt the material parameter for bolts consisting of solid elements suitable for use in large vehicle crash simulations with LS-DYNA. Specially designed test setups provide the data to adjust the material parameter for an isotropic material model combined with the phenomenological damage model GISSMO (**G**eneralized **I**ncremental **S**tress-**S**tate dependent damage **MO**del) [9]. Based on tensile and shear tests, a three-dimensional fracture locus defines the plastic fracture strain depending on the triaxiality η and the Lode parameter ξ. This failure surface is shaped according to the approach suggested by Bai and Wierzbicki [10] and is adjusted to a fine-meshed model with an average element length of 0.5 mm. A regulation factor reduces the plastic fracture strain consistently and makes it applicable for a coarse-meshed bolt model with an average element length of 2.5 mm. A comparison of the results points out the numerical restrictions due to the discretization size of the fine and coarse-meshed model.

2 Experiments

Fig. 1 shows the experimental setups used in the investigations on the bolt's failure behavior. The setups convert a load acting form above into a tension load as shown in Fig. 1 a), a shear load as shown in Fig. 1 b) or a combined load as shown in Fig. 1 c). All parts are oversized to cause a failure exclusively in the bolt. This enables the usage in a drop tower to observe the failure behavior under dynamic loads. The physical references shown in section 5 are generated with a quasi-static velocity.
The most important insight of the tensile tests is the variation of the fracture strain depending on the shank to thread ratio. Stiffness, strength and elongation are varying under shear when comparing shaft and thread in the shear joint. Schauwecker et al. [6] describe the insights of the experimental investigation in detail.

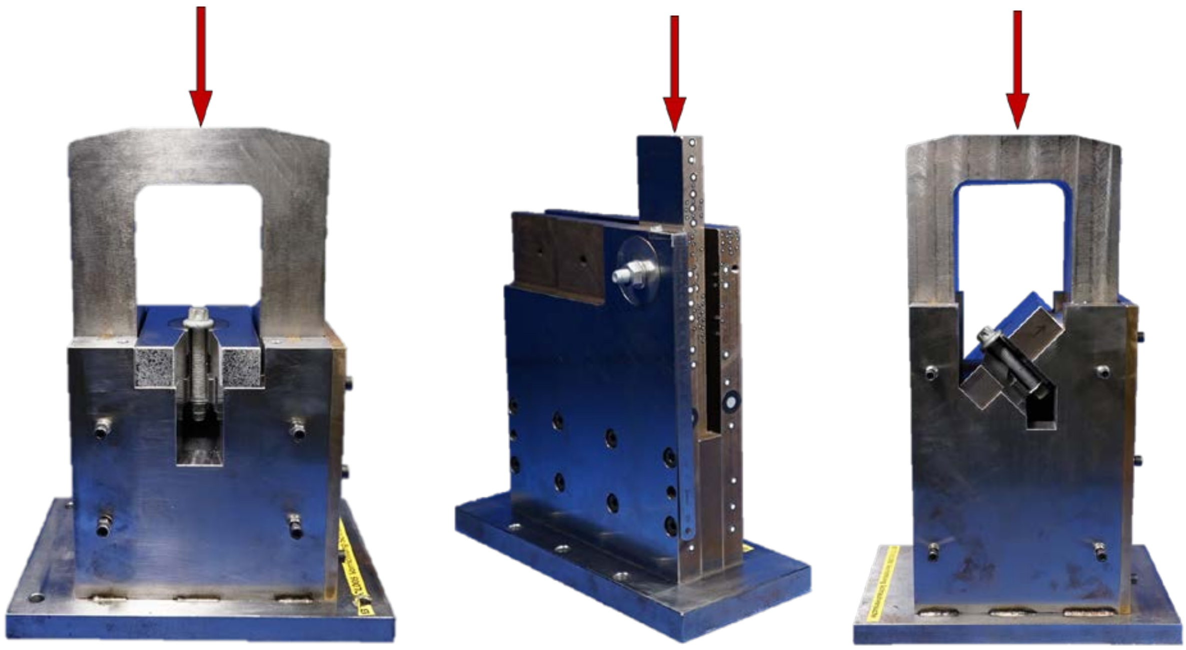

a) Tension setup *b) Shear setup* *c) Setup for combined load*

Fig.1: Experimental setups

3 Constitutive Model

The isotropic constitutive model **`*MAT_PIECEWISE_LINEAR_PLASTICITY (*MAT_24)`** uses the yield curve obtained from the tensile test. To generate this yield curve, the engineering stress and strain values are transformed into the true stress and strain values up to the necking point. Beyond the necking point, the Hockett-Sherby [11] approach extrapolates the yield curve. Fig. 12 in section 5 shows the adjustment of the yield curve for a fine-meshed bolt model and Fig. 14 illustrates the same for a coarse-meshed model. Damages and failure are exclusively considered by the GISSMO model which is applied to the constitutive model over an additional option **`*MAT_ADD_EROSION`**. GISSMO calculates the failure over a strain-based criterion depending on the elements stress state. For shell elements with a plane stress assumption, the stress state is unambiguously defined by the stress triaxiality η. Solid elements have, however, a three-dimensional stress state. Thus, the deviatoric state variable or Lode angle parameter ξ and the stress triaxiality are independent of each other which is why the fracture strain is depending on both parameters. Equation (1) defines the triaxiality as the mean stress σ_m divided by the von Mises stress σ_{vM}. The Parameter I_1 is the first invariant of the Cauchy stress tensor. The Lode angle parameter is defined in equation (2) with J_3 as the third invariant of the deviatoric stress tensor.

$$\eta = \frac{\sigma_m}{\sigma_{vM}} = \frac{1}{3}\frac{I_1}{\sigma_{vM}} \tag{1}$$

$$\xi = \frac{27}{2}\frac{J_3}{\sigma_{vM}^3} \qquad \text{with} \qquad J_3 = s_1 s_2 s_3 \tag{2}$$

Fig. 2 shows a characteristic failure surface of the plastic fracture strain ε_f according to Bai and Wierzbicki [10]. This asymmetric surface is defined with three curves suggested by Johnson and Cook [12] in the equations (3) to (5) at constant Lode angle parameters (ξ = 1, ξ = 0 and ξ = -1). In addition, these three curves are connected to create a surface by the quadratic approach of Bai and Wierzbick [10] in equation (6).

$$\varepsilon_f^+(\eta) = D_1 + D_2^{-D_3\eta} \qquad \text{for} \qquad \xi = 1 \tag{3}$$

$$\varepsilon_f^0(\eta) = D_4 + D_5^{-D_6\eta} \qquad \text{for} \qquad \xi = 0 \tag{4}$$

$$\varepsilon_f^-(\eta) = D_7 + D_8^{-D_9\eta} \qquad \text{for} \qquad \xi = -1 \tag{5}$$

$$\varepsilon_f(\eta,\xi) = \left[\frac{1}{2}\left(\varepsilon_f^-(\eta) + \varepsilon_f^+(\eta)\right) - \varepsilon_f^0(\eta)\right]\xi^2 + \frac{1}{2}\left(\varepsilon_f^+(\eta) - \varepsilon_f^-(\eta)\right)\xi + \varepsilon_f^0(\eta) \tag{6}$$

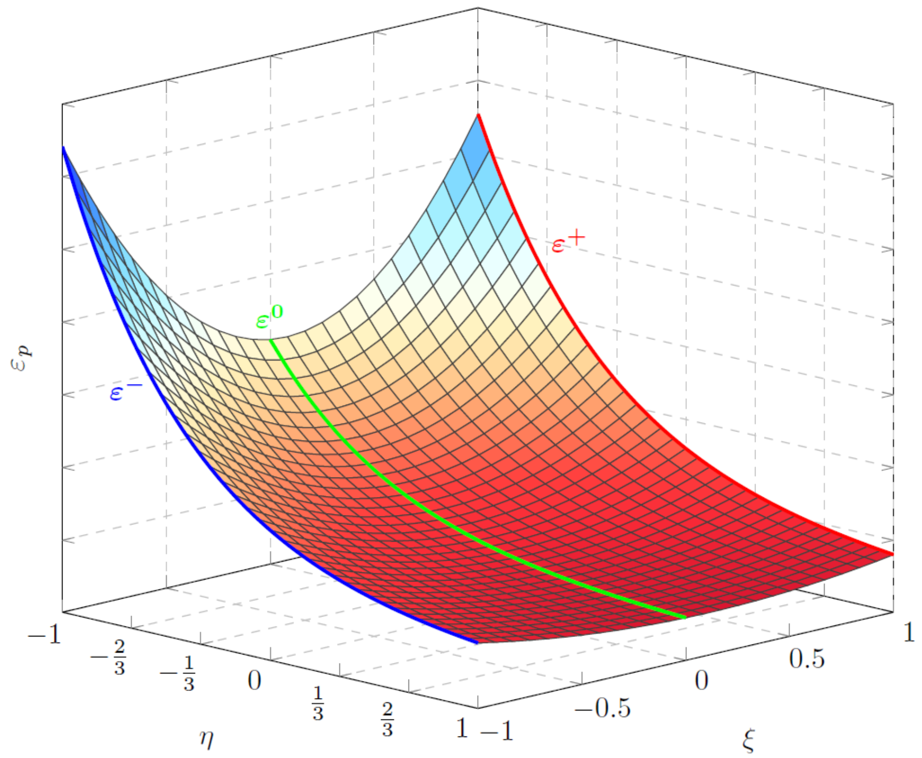

Fig.2: Characteristic failure surface of the plastic fracture strain according to Bai and Wierzbicki [10]

Bai and Wierzbicki's approach allows the definition of a failure surface based on nine parameters (D_1, D_2, …, D_9). Since only two experimental results are available, certain assumptions have to be made to complete the remaining parameters. Fig. 3 shows the characteristic failure surface of the bolt material after implementing the following assumptions.
For high triaxialities, the difference among the three curves becomes negligibly small. The assumption that all three curves converge to the same fracture strain in infinity eliminates already two parameters. As a high-strength steel, the CP 1000 steel has similar material properties as a 10.9 bolt. Its fracture strain for high triaxialities is thus regarded as an appropriate value. Furthermore, it is assumed that the curves are identical for ξ = 1 and ξ = -1 (i.e. $\varepsilon^+ = \varepsilon^-$) due to the lack of information for the ξ = -1 curve. This assumption makes the surface similar to the approach of Wierzbicki and Xue [13] and omits two further parameter. Failure is not expected at triaxialities below η = -⅔, hence the fracture strain is on a constant high level for η =< -⅔. The transition is continuous for ξ = 1 and ξ = -1 at η = -⅔. For the

curve for ξ=0 is the fracture strain reduced at η = -⅔ to keep the concave shape of the failure surface. The remaining two parameters are adapted to the results of the experimental investigations. The fracture strains at η = 0, ξ = 0 and η = ⅓, ξ = 1 are adjusted according to the shear and tensile tests respectively.
The adjustment of the material card, and thus the plastic fracture strain surface in Fig. 3, bases on the results of the fine-meshed model. A regulation factor consistently reduces the fracture strains to ensure that the material card fits an average element length of 2.5 mm.

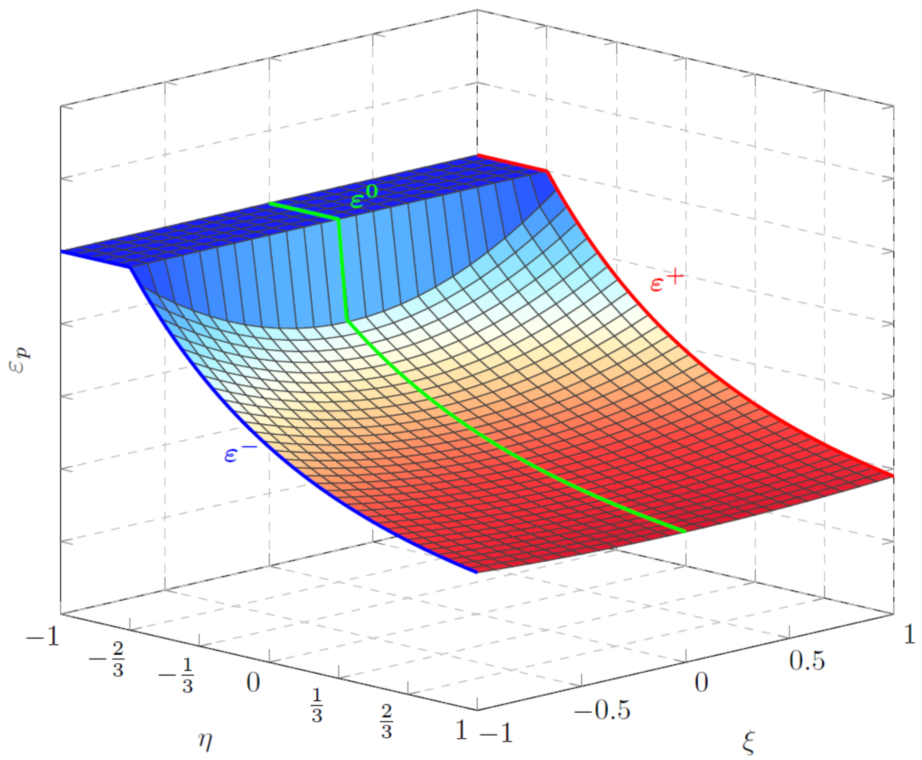

Fig.3: Failure surface of the fracture strain adapted to the results of the bolt failure investigations

Neukamm [9] provides more detailed information about the calibration, validation and the development of the GISSMO damage model. He focuses on the application in thin sheet metal structures in which a plane stress can be assumed.
Basaran [14] describes the extension of the GISSMO model for volumetric elements in which three-dimensional stress states can be described. His work focuses on the influence and dependency of the Lode angle parameter.

4 Numerical Models

4.1 Fine Numerical Model

The fine-meshed numerical models of the three different load cases are shown in Fig. 4. Schauwecker et al. [6] describe in detail the tensile model in Fig. 4 a) and the shear model in Fig. 4 b). The combined load model in Fig. 4 c) uses the periphery of the tensile model with a change in the boundary conditions.
A local coordinate system, which is turned by 45°, defines the displacement direction. The joining part nodes are each connected to a beam element in the center of gravity of the respective component. Both beams use a conventional steel material card and have an oversized diameter of 1000 mm to keep the elongation of the beams negligibly small. The free end of the upper beam is constrained in all translational and rotational degrees of freedom while a constant displacement is applied in local Z direction to the free end of the lower beam. Both beams use the element formulation 9 with the material model **`*MAT_SPOTWELD`** (**`*MAT_100`**) which enables to measure the forces in the system.

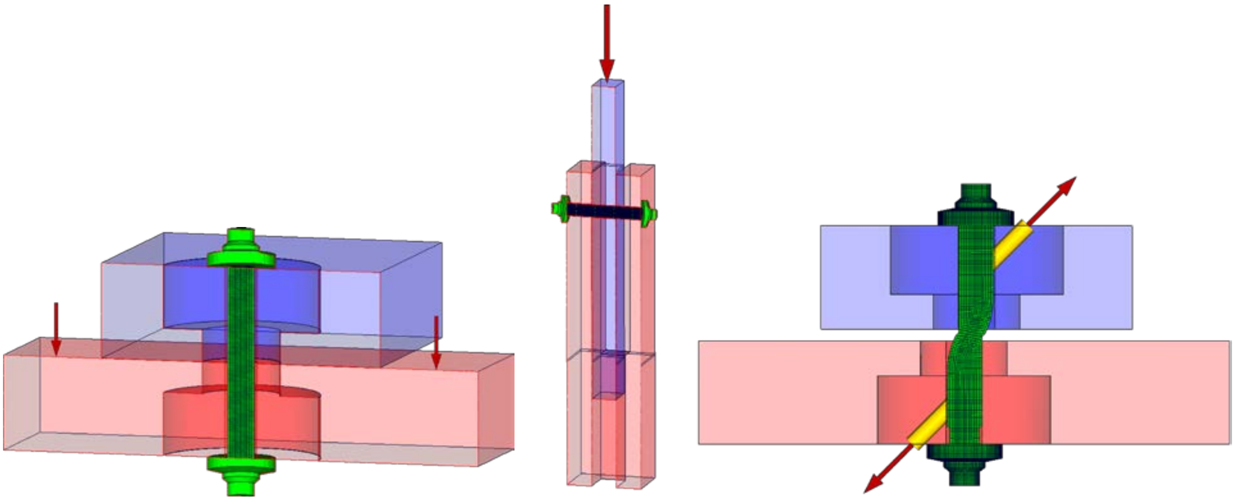

a)Tension model *b) Shear model* *c) Model for combined load*

Fig.4: Fine-meshed model setups

Fig. 5 shows the fine-meshed bolt model compared to a real bolt. A reduction of the diameter distinguishes between the thread and the shank. The shank is one element row thicker than the thread to reach the nominal diameter. With a mesh size of 0.5 mm, the discretization is fine enough to investigate the bolt's principle physical behavior. However, the discretization is still not fine enough to precisely depict the thread geometry and thus it shows the numerical limitations of a mesomechanical approximation.
Fig. 6 illustrates the distribution of the elements over the cross section.

Fig.5: Fine-meshed bolt model compared to a real bolt

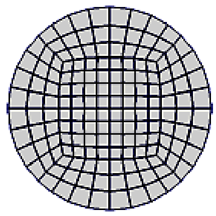

Fig.6: Cross section of the fine-meshed bolt model

4.2 Coarse Numerical Model

The coarse discretized numerical model corresponds to the fine-meshed model and uses an average element length of 2.5 mm. Fig. 7 illustrates the coarse-meshed models of the respective load cases.

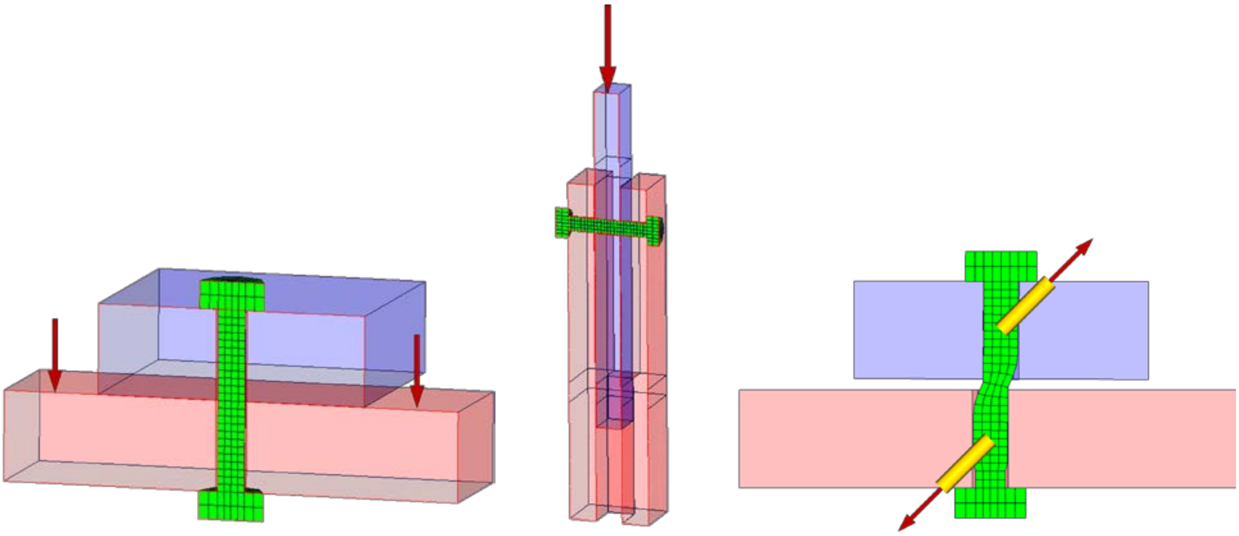

a) Tension model *b) Shear model* *c) Model for combined load*

Fig.7: Coarse-meshed model setups

The geometry of the coarse bolt modeling is shown in Fig. 8 and Fig. 9. In contrast to the fine-meshed model, the transition between the shank and the thread cross section takes place over the distance of an element row. Fig. 10 shows the cross section of a coarse-meshed bolt.

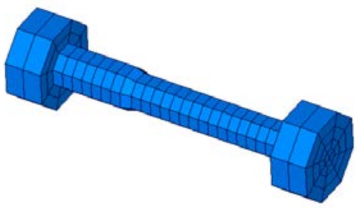

Fig.8: Coarse-meshed bolt model

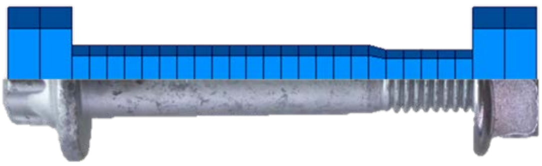

Fig.9: Coarse-meshed bolt model compared to a real bolt

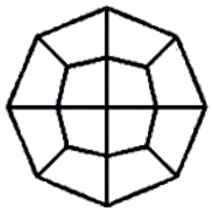

Fig.10: Cross section of a coarse-meshed bolt model

Schauwecker et al. [7] emphasize the importance of the surface area between an octagon and a circle with the same diameter. Some substitute models use the nominal bolt diameter for the entire shank and thread. This makes the cross-sectional area of the thread larger than the actual one, while the cross-sectional area of the shank becomes smaller. In a physically correct model, the cross-sectional areas of the model correspond to the cross-sectional areas of the real bolt.

5 Results and discussion

5.1 Tension (without failure)

The results in Fig. 12 show the behavior of the material in the tensile test without taking damage and failure into account – only the yield curve affects the behavior. The simulation result matches the physical test almost until failure. As no failure is active, the necking continues until the end of the calculation. Close to fracture, the simulation result deviates from the experimental curve, when the elements deform excessively. At this point the element size reaches its limits.
Fig. 11 shows the plastic strain distribution of the fine-meshed model. The plastic strains appear in the elements around the necking area while the rest of the bolt deforms mainly elastic. Two rows of elements in the middle are deforming more than the surrounding ones.

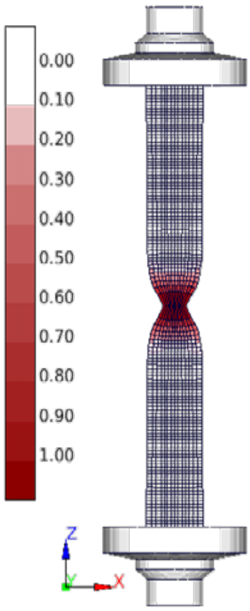

Fig.11: Maximum plastic strains of the fine-meshed model under tensile load without damage

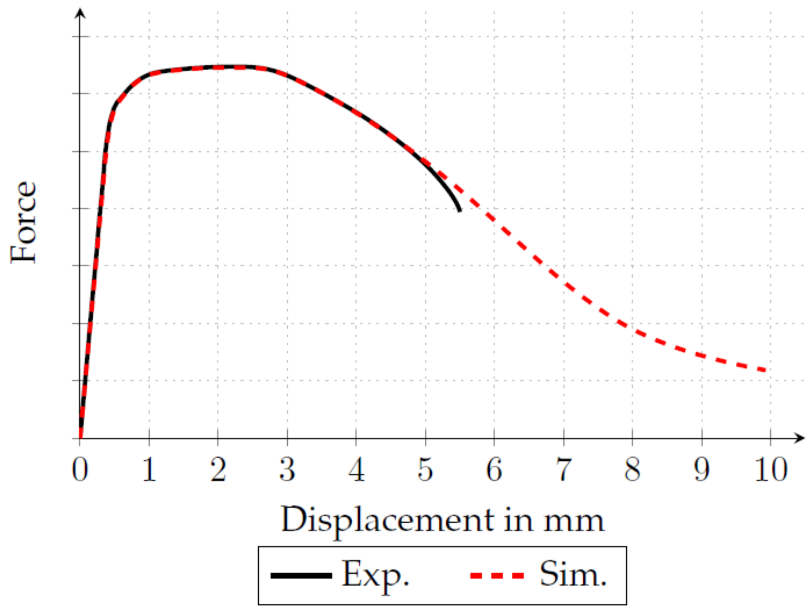

Fig.12: Force-displacement diagram of the fine-meshed model under tensile load without taking damage into account

Fig. 13 depicts the plastic strain distribution of the coarse-meshed model under tensile load. As the picture shows, most plastic deformation takes place over two element rows. These two element rows should represent the same deformation as the fine-meshed model, in which the plastic strains are distributed over ten element rows. The coarse modeling leads to an earlier divergence between the numerical result and the physical test, as seen in the force displacement diagram in Fig. 14.

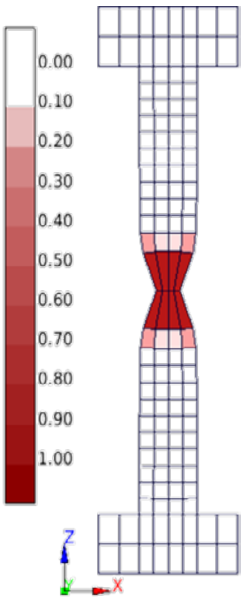

Fig.13: Maximum plastic strains of the coarse-meshed model under tensile load without damage

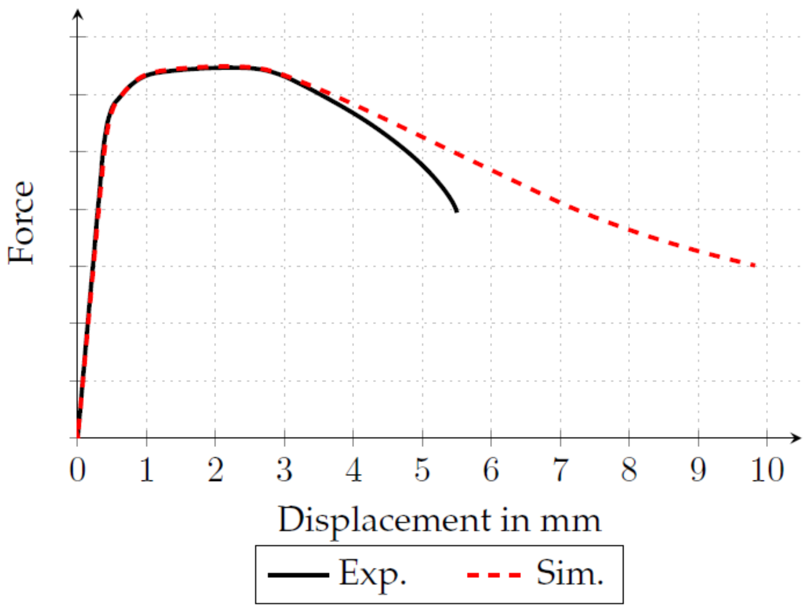

Fig.14: Force-displacement diagram of the coarse-meshed model under tensile load without taking damage into account

5.2 Tension (with failure)

Fig. 16 shows the force-displacement diagram of the tensile test with an adapted material card considering the damage via GISSMO. The distribution of the triaxiality in the bolt's longitudinal cross section right before failure is indicated in Fig. 15. When plastic deformation starts, the triaxiality of the elements in the necking area exceed η = ⅓ while the elements have negative triaxialities below and above the necking area.

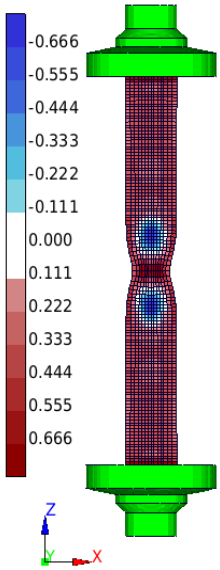

Fig.15: Triaxiality of the fine-meshed bolt model under tension

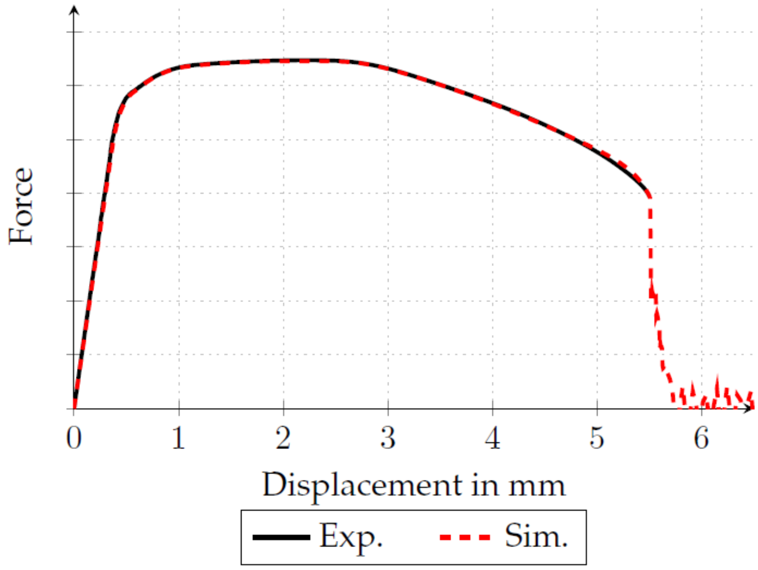

Fig.16: Force-displacement diagram of the fine-meshed model under tension

As illustrated in Fig. 17, the elements show a similar characteristic triaxiality distribution as the fine-meshed bolt model. However, the resolution is not fine enough to capture the same triaxiality values. This is the reason why the fracture strains need to be reduced. Fig. 18 shows the force-displacement progress and also that the bolt fails at the same elongation but at a lower force level compared to the experiment. A perfect correspondence would be possible with a further calibration of the material card for this specific element size, geometry and loading condition.

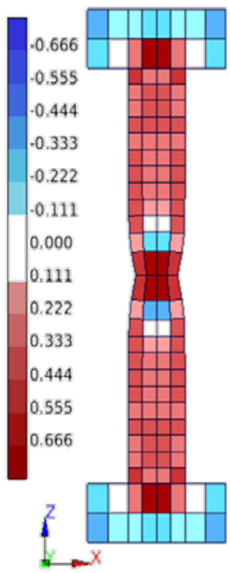

Fig.17: Triaxiality of the coarse-meshed bolt model under tension

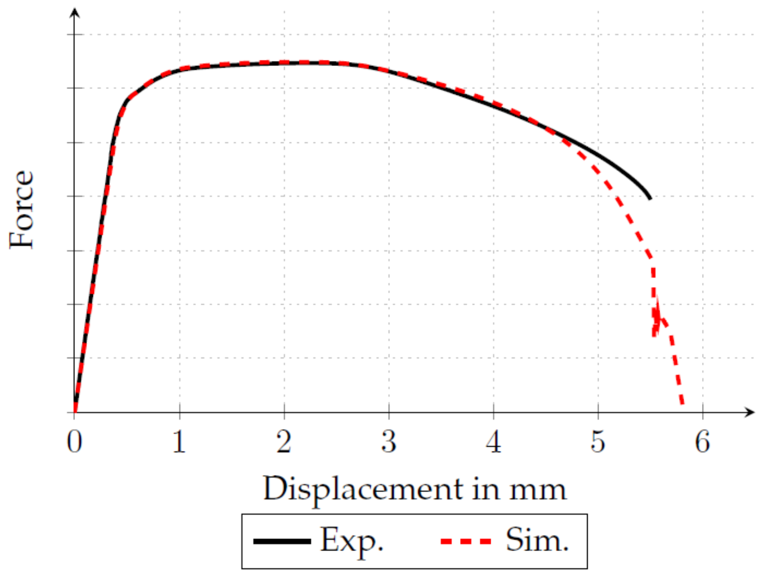

Fig.18: Force-displacement diagram of the coarse-meshed model under tension

5.3 Shear (with failure)

Fig. 19 shows a cut through the fine-meshed bolt model under shear right before the first element fails. The elements in the gap start with a pure shearing triaxiality around $\eta = 0$ and move to positive triaxiality values still bellow $\eta = ⅓$ with increasing deformation. Fig. 20 shows the elements in the shear joint in a close-up view. The Lode angle parameter is between $\xi = -0.5$ and $\xi = 0.5$ for those elements.
The force-displacement diagram in Fig. 21 shows the results of shearing through the shank and through the thread. Both cases reach almost the same force level as their corresponding physical test. The absorbed energy for shearing through the shank is equal to the energy of the experimental result. Under shearing through the thread, the diagram shows that the effect of the compressed thread, presented in section 2, cannot be simulated with this type of modeling. Consequently, this leads to a discrepancy in the stiffness and total elongation.

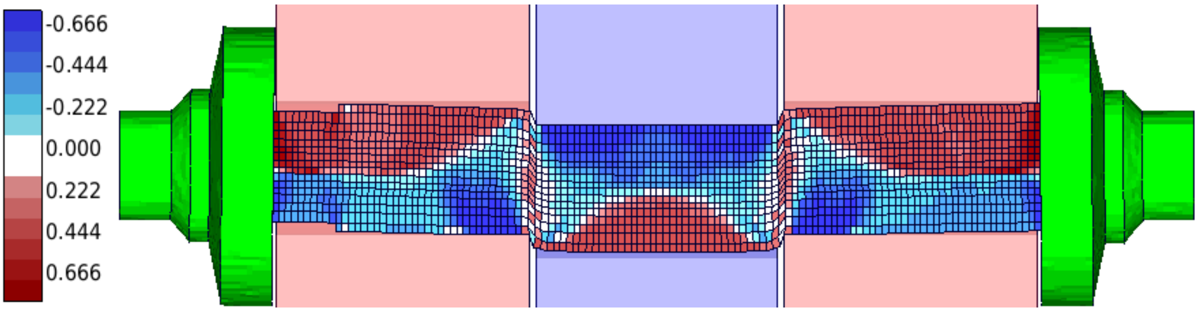

Fig.19: Triaxiality of the fine-meshed bolt model under shear

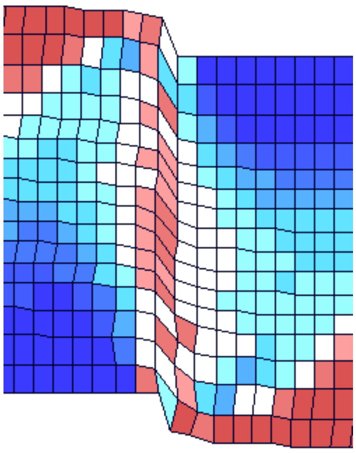

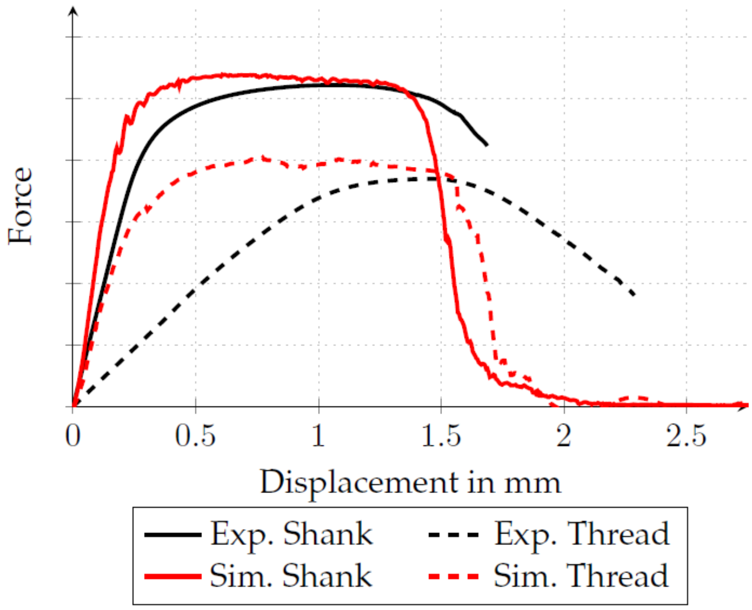

Fig.20: Close-up view of Fig. 19

Fig.21: Force-displacement diagram of the fine-meshed model under shearing through the shank and the thread

Fig. 22 depicts the triaxiality distribution of the coarse-meshed model under shear right before the first element fails. In the beginning of the simulation, the elements are compressed due to the large element size and the close shear gap of 0.5 mm. The range of the triaxiality is varying from values below $\eta = -⅔$ to values beyond $\eta = 0$. Therefore, it is important that the fracture strains below $\eta = -⅔$ are not chosen too high, since the damage accumulation will be too low and the elements will deform even further without failing. Fig. 23 shows the elements in the shear joint in a close-up view. Here, the element edge is exactly in the middle of the shear joint, representing the ideal case. Results with an element across the shear joint reach even higher force levels than the results of the idealized case shown in the force-displacement diagram in Fig. 24.

The maximum force in the simulation results is around 40% higher than the maximum experimental force, whereas the elongation is twice as high. Furthermore, the elongation could be reduced with a further calibration of the fracture strain which, however, would not noticeably affect the force level.
In comparison to the fine-meshed model, four elements are too coarse to precisely capture the actual material behavior as well as the damage evolution under shear.

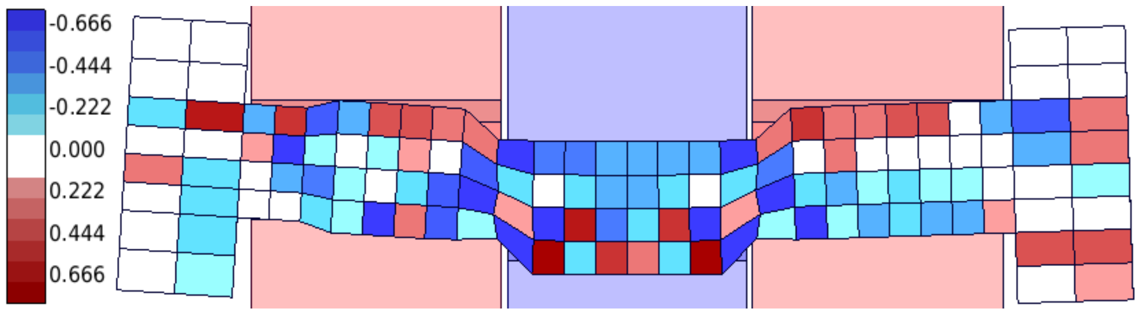

Fig.22: Triaxiality of the coarse-meshed bolt model under shear

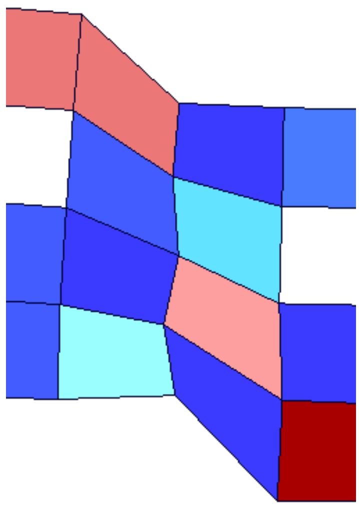

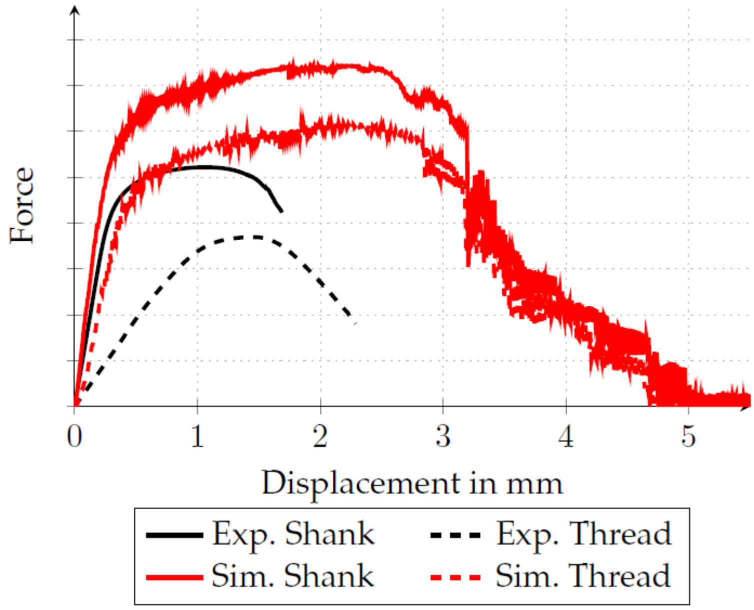

Fig.23: Close-up view of Fig. 22

Fig.24: Force-displacement diagram of the coarse-meshed model under shearing through the shank and the thread

6 Summary

This paper presents a method for the calibration of an isotropic constitutive law coupled with the phenomenological damage model GISSMO applicable to bolt models for full vehicle crash simulations consisting of solid elements. Specially designed experimental setups are used for the calibration of the yield curve for the isotropic constitutive law. A three-dimensional failure surface defines the fracture strains in dependence of triaxiality and Lode angle according to Bai and Wierzbicki's [10] approach. The limitation of experimental results makes some assumptions necessary which are described in this paper. The numerical results of the fine-meshed model show good agreement to the experiment under tensile load and an equivalent energy absorption under shear through the bolt shank. Furthermore, a comparison between a fine-meshed and a coarse-meshed model shows the limits of a coarse discretization which is insufficient to properly describe the actual deformation. Typical full car crash models demand element sizes which provide an acceptable computational solution time. Nowadays, this is the case for mesh sizes around 3 mm. Therefore, the results of the presented study for an element size of 2.5 mm are currently considered to be a good compromise between computational efficiency and numerical accuracy.
Finally, the experimental setup as well as its numerical representation for combined tensile and shear loads under 45° validates the quality of the calibrated material card.

7 Literature

[1] U. Sonnenschein, Modelling of bolts under dynamic loads, 7. LS-DYNA Anwenderforum, Bamberg, 2008

[2] S. Narkhede, N. Lokhande, B. Gangani, G. Gadekar, Bolted Joint Representation in LS-DYNA to Model Bolted Pre-Stress and Bolt Failure Characteristics in Crash Simulations, 11th International LS-DYNA Users Conference, Dearborn MI USA, 2010

[3] M. Hadjioannou, D. Stevens, M. Barsotti, Development and Validation of Bolted Connection Modelling in LS-DYNA for Large Vehicle Models, 14th International LS-DYNA Users Conference, Detroit MI USA, 2016

[4] H. Franzplass, M. Langseth, O. S. Hopperstad, Experimental and numerical study of threaded steel fasteners under combined tension and shear at elevated loading rates, International Journal of Impact Engineering, 2015

[5] H. Franzplass, M. Langseth, O. S. Hopperstad, Numerical study of the tensile behavior of threaded steel fasteners at elevated rates of strain, International Journal of Impact Engineering, 2013

[6] F. Schauwecker, D. Moncayo, M. Beck, P. Middendorf, Investigation of the Failure Behavior of Bolted Connections under Crash Loads and a Novel Adaption to an Enhanced Abstracted Bolt Model, 15th International LS-DYNA Conference, Detroit, Michigan, USA, 2018

[7] F. Schauwecker, D. Moncayo, M. Beck, P. Middendorf, Investigation of the Predictive Ability of Idealized Bolt Models for Large Vehicle Simulations under Crash Loads, 18 Dach Conference, Bamberg, 2018

[8] International standard, ISO 898-1, mechanical properties on fasteners made of carbon steel and alloy steel – Part 1: bolts, screws and studs, Brussels: European Committee for Standardization, 1999

[9] F. Neukamm, Lokalisierung und Versagen von Blechstrukturen: Dissertation, Vol. Nr. 68 of Bericht / Institut für Baustatik und Baudynamik der Universität Stuttgart, Stuttgart, 2018. doi:10.18419/opus-10082.

[10] Y. Bai, T. Wierzbicki, A new model of metal plasticity and fracture with pressure and Lode dependence, International Journal of Plasticity 24 (6) (2008) 1071 - 1096. doi:10.1016/j.ijplas.2007.09.004.

[11] J. E. Hockett, O. D. Sherby, Large strain deformation of polycrystalline metals at low homologous temperatures, Journal of the Mechanics and Physics of Solids 23 (2) (1975) 87-98. doi:10.1016/0022-5096(75)90018-6

[12] G. R. Johnson, W. H. Cook, Fracture characteristics of three metals subjected to various strains, strain rates, temperatures and pressures, Engineering Fracture Mechanics 21 (1) (1985) 31-48. doi:10.1016/0013-7944(85)90052-9.

[13] Wierzbicki T, Xue L On the effect of the third invariant of the stress deviator on ductile fracture. Technical report, Impact and Crashworthiness Laboratory, Massachusetts Institute of Technology, Cambridge, MA

[14] M. Basaran, Stress state dependent damage modeling with a focus on the lode angle influence, Berichte aus dem Maschinenbau, Shaker, Aachen, 2011.